Applied Physics Letters

Dependence of the coupling properties between a plasmonic antenna array and a sub-wavelength epsilon-near-zero film on structural and material parameters

Cite as: Appl. Phys. Lett. **118**, 241102 (2021); https://doi.org/10.1063/5.0042599
Submitted: 01 January 2021 . Accepted: 24 May 2021 . Published Online: 14 June 2021

Karapet Manukyan, M. Zahirul Alam, Cong Liu, Kai Pang, Hao Song, Zhe Zhao, Moshe Tur, Robert W. Boyd, and Alan E. Willner

Applied Physics Letters ARTICLE scitation.org/journal/apl

Dependence of the coupling properties between a plasmonic antenna array and a sub-wavelength epsilon-near-zero film on structural and material parameters

Cite as: Appl. Phys. Lett. **118**, 241102 (2021); doi: 10.1063/5.0042599
Submitted: 1 January 2021 · Accepted: 24 May 2021 ·
Published Online: 14 June 2021

Karapet Manukyan,[1,a)] M. Zahirul Alam,[2] Cong Liu,[1,3] Kai Pang,[1] Hao Song,[1] Zhe Zhao,[1] Moshe Tur,[4] Robert W. Boyd,[2,5] and Alan E. Willner[1]

AFFILIATIONS

[1]Department of Electrical Engineering, University of Southern California, Los Angeles, California 90089, USA
[2]Department of Physics, University of Ottawa, Ottawa, Ontario K1N 6N5, Canada
[3]Department of Physics and Astronomy, University of Southern California, Los Angeles, California 90089, USA
[4]School of Electrical Engineering, Tel Aviv University, Ramat Aviv 69978, Israel
[5]The Institute of Optics, University of Rochester, Rochester, New York 14627, USA

Note: This Paper is part of the APL Special Collection on Metastructures: From Physics to Applications.
[a)]**Author to whom correspondence should be addressed:** kmanukya@usc.edu

ABSTRACT

The resonance properties of a plasmonic dipole antenna array depend on its geometry and the properties of its surrounding medium. The linear optical properties of an array of plasmonic dipole antennas can be modified with the inclusion of an epsilon-near-zero (ENZ) thin film. In this work, we numerically investigate the roles of the antenna dimensions, the ENZ film thickness and loss, and the separation between the antenna and the ENZ film in determining the linear optical response of the antenna–ENZ metasurface. The results show that for a sufficiently small separation, the linear optical properties of the antenna array are determined by the strong or ultrastrong coupling with the ENZ film and are only weakly dependent on the antenna geometry. We show that for metasurfaces with thick, lossy ENZ films, the lower polariton branch is not observable due to the high loss of ENZ films. Since the dependence of the upper polariton on antenna length is weak, this results in a single antenna-length-invariant resonance. However, in the presence of low-loss ENZ films, the lower polariton branch is also visible for antenna–ENZ metasurfaces with thicker ENZ films, indicating a strong coupling between the antenna array and the ENZ film. For a given antenna geometry, the coupling strength increases with increasing thickness of the ENZ film and can reach up to ∼50% of the zero-permittivity frequency of the ENZ film, indicating an ultrastrong coupling between the plasmonic antenna array and the ENZ film.

Epsilon-near-zero (ENZ) materials have gained much interest due to their potentially unusual linear optical response and large nonlinearity.[1–10] Specifically, it has been reported that transparent conducting oxides such as indium tin oxide (ITO) and aluminum doped zinc oxide (AZO) exhibit large nonlinear optical responses in the near-infrared wavelength regions.[2,3,5,6,8,9]

A number of recent works have pointed toward unique linear and enhanced nonlinear light–matter interactions of ENZ materials coupled with plasmonic nanoantenna arrays.[11–22] Particularly, there have been multiple observations of strong-coupling-induced resonance splitting of an antenna array's fundamental resonance in the presence of a thin ENZ film, resulting in two spectrally separated distinct resonances at shorter (upper polariton) and longer (lower polariton) wavelengths.[11,12,14–20] "Strong coupling" is the interaction regime in which the spectral separation of the upper and lower polaritons of the coupled system is of the same order of magnitude as the linewidth of each uncoupled resonance. The strong antenna-ENZ coupling results in a strong field enhancement inside the ENZ film and makes the effective refractive index of the metasurface highly tunable, potentially enabling several applications.[14,23–27] Furthermore, transitioning from a strong coupling to an "ultrastrong coupling" regime, in which the resonance splitting is of the same order of magnitude as the

zero-permittivity frequency of the ENZ film, further enhances the efficiency of the antenna–ENZ interactions, potentially enabling even more applications.[23–28]

The effect of strong antenna–ENZ coupling-induced resonance splitting was demonstrated for metasurfaces with subwavelength ENZ films.[12,14] It has also been shown that the presence of an ENZ film leads to antenna-length-invariant resonances of antenna-ENZ metasurfaces (i.e., resonance pinning).[21,22] To engineer such strongly coupled antenna–ENZ metasurfaces, it might be of interest to explore the role of structural and material parameters on the antenna–ENZ coupling strength. In this work, we explore the following additional issues: (a) the dependences of the coupling strength between the antenna array and the ENZ film on the structural and material parameters, such as the ENZ film thickness and loss, antenna–ENZ separation, antenna length; (b) the conditions required to achieve an ultrastrong coupling regime between the antenna array and the ENZ film; and (c) the connection between the phenomena of strong coupling and resonance pinning in antenna–ENZ metasurfaces.

In this paper, we show by simulation that with a sufficiently small separation between the antenna array and the ENZ film, the ENZ film and the metallic antenna array are in a strong or ultrastrong coupling regime. The loss of the ENZ film largely weakens the lower polariton resonance of the metasurface, making it undetectable for thicker ENZ films with large loss, resulting in a single resonance at a shorter wavelength. This resonance is weakly dependent on antenna length due to the resonance pinning effect.[21,22] We also show that decreasing the loss of the ENZ film does not increase the coupling strength but makes the metasurface resonances stronger. Consequently, the lower polariton branch becomes visible for metasurfaces with thicker ENZ films too, showing a large splitting of upper and lower polariton resonances and indicating a strong antenna–ENZ coupling. The coupling becomes stronger as the ENZ film thickness increases, with the resonance splitting reaching up to 50% of the zero-permittivity frequency of the ENZ film and saturating in an ultrastrong coupling regime.

Figure 1(a) shows the structure of the finite-difference-time-domain (FDTD) simulation model: a SiO_2 layer serves as the substrate for the metasurface. An array of periodic gold antenna bars is placed on top of the ITO–ENZ film. We vary the thickness of the ITO film in the range of 0–300 nm. The unit cell size of the antenna array and the width and the thickness of the antenna are fixed to 800, 100, and 40 nm, respectively. The polarization of the normal incidence electric field is along the long axis of the antenna. A commercially available software, Lumerical FDTD solutions, was used for the simulations. A broadband source was used in simulation to calculate the transmittance of the metasurface. The unit cell size is fixed, and the structure is assumed to be periodic as the boundary conditions of the unit cell. We use experimentally measured permittivity data of a 23 nm-thick ITO film obtained by ellipsometry in our simulations [Fig. 1(b)]. The real part of the permittivity Re(ε) crosses zero at the zero-permittivity wavelength of $\lambda_{ENZ} = 1360$ nm. The imaginary part of the permittivity Im(ε) is non-zero and corresponds to the absorption loss of the ITO film. An ITO film supports a longitudinal bulk-plasma mode and surface plasmon-polariton (SPP) modes at both interfaces.[1,29–31] For film thicknesses comparable to the skin depth, SPP modes of two interfaces couple producing long-range (LR) and short-range (SR) SPP modes.[1,30,31] In a thin ENZ film, the LR–SPP mode exists near the ENZ wavelengths and is known as the ENZ mode.[1] Figure 1(c) shows

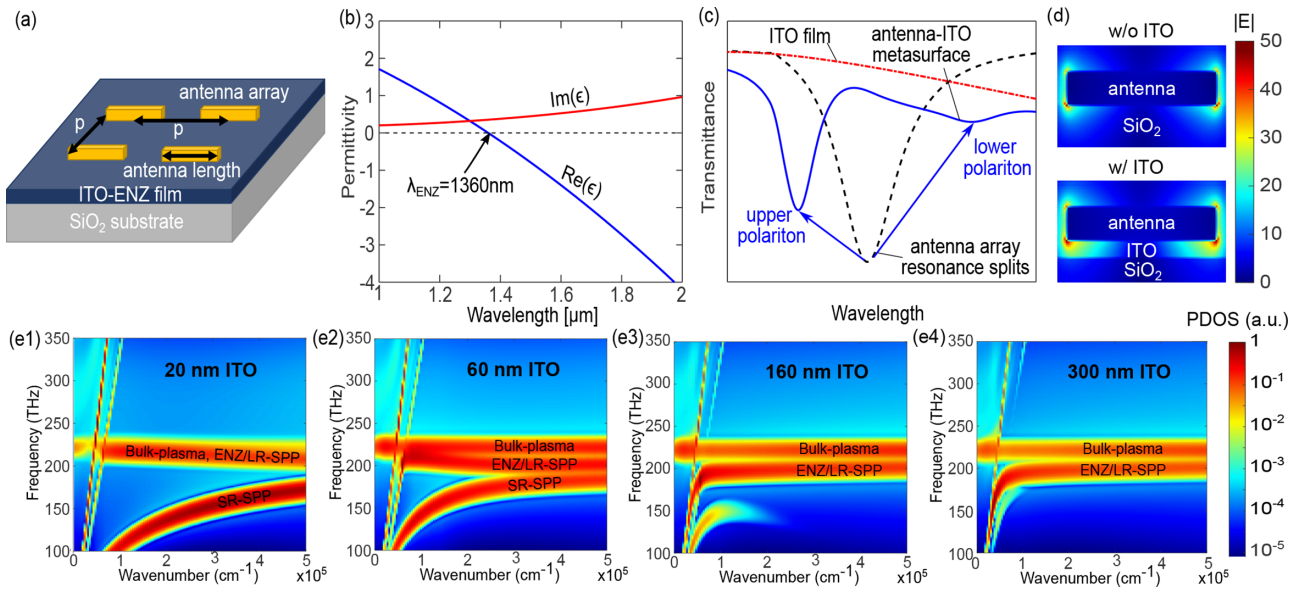

FIG. 1. The concept of the simulation model. (a) The structure of the antenna–ITO metasurface. The ITO–ENZ film is on a thick SiO_2 substrate. An array of gold nanobars is on top of the ITO–ENZ film. (b) The real (blue) and imaginary (red) parts of the measured permittivity data of the ITO–ENZ film used in the simulations. The real part of the permittivity is zero at λ_{ENZ}=1360 nm. (c) The transmittance of the ITO film (red), the gold antenna array (black), and the antenna–ITO metasurface (blue). The interaction between the antenna array and the ITO–ENZ film results in splitting of the fundamental resonance of the antenna array, with the splitting amount indicating the coupling strength. (d) The field distribution along the antenna near its edge without and with an ITO–ENZ film. (e1)–(e4) Dispersion diagrams of ITO–ENZ films of 20, 60, 160, and 300 nm thicknesses, respectively.

the transmittance curves of the antenna–ITO metasurface, the antenna array, and the pure ITO film. The transmittance of the structures is investigated compared to the transmittance in free space, where unity transmittance corresponds to the transmittance in vacuum. The dipole plasmonic mode of the antenna and the ENZ mode of the ITO couple strongly, leading to the splitting of the fundamental resonance of the antenna into upper and lower polariton branches of the antenna–ITO metasurface.[11,14] Figure 1(d) shows the field distribution along the antenna near its edge without and with an ITO–ENZ film. The presence of the ITO–ENZ film leads to a strong field enhancement inside the ITO due to the strong antenna–ITO coupling. Figures 1(e1)–1(e4) show the dispersion diagrams of ITO films of 20, 60, 160, and 300 nm thicknesses, respectively. We calculate the dispersion by calculating the photonic density of states (PDOS) of ITO films using complex frequencies and real wavenumbers. For an ITO film of 20 nm thickness, the LR–SPP mode merges with the bulk-plasma mode and has a flat dispersion profile. When increasing the ITO film thickness to 300 nm, the LR–SPP mode separates from the bulk-plasma mode of the ITO film but still remains in the vicinity of the ENZ region. Thus, for the thickness range studied in this paper, we refer to LR–SPP of the ITO film as the ENZ mode. We explore the ratio g of the frequency separation between the upper and lower polariton resonances and the zero-permittivity frequency of the ITO–ENZ film,

$$g = \frac{\omega_g}{\omega_0} = \frac{\Delta\omega}{\omega_0}, \tag{1}$$

as an indicator of the coupling strength between the antenna array and the ITO–ENZ film under different metasurface parameters,[23,24,27,28] where $\omega_g \equiv \Delta\omega$ is the frequency difference between the upper and lower polaritons, and ω_0 is the frequency of the zero-permittivity of the ITO film.

First, we explore the dependence of the antenna–ENZ coupling on the thickness of the ITO–ENZ film of the metasurface. Figure 2(a) shows the transmittance of ITO films with thicknesses of 70, 120, and 200 nm, and Fig. 2(b) shows the transmittance of antenna–ITO metasurfaces with ITO thicknesses of 10, 70, and 120 nm, respectively. The black curve corresponds to the transmittance of the antenna array without the ITO film. The length of the antenna is fixed at 320 nm. As shown in Fig. 2(b), the presence of the ITO film as thin as 10 nm results in a splitting $\Delta\lambda$ of the fundamental resonance of the antenna of ~300 nm, leading to two distinct resonances of the antenna–ITO metasurface. The splitting increases to $\Delta\lambda \sim 600$ nm for the metasurface with 70 nm thickness of ITO. However, for the metasurface with a 120 nm ITO thickness, the lower polariton is no longer observable due to the loss of the film. Figure 2(c) shows the dependence of the resonance wavelengths of the upper and lower polaritons of the antenna–ITO metasurface with ITO thicknesses of 10 and 80 nm as a function of the antenna length. We find that for the 10-nm-thick ITO, the splitting $\Delta\lambda$ is >265 nm. This amount of resonance separation is greater than the linewidth of the antenna resonance, indicating a strong antenna–ENZ coupling. For the metasurfaces with the 80-nm-thick ITO, the resonance separation $\Delta\lambda$ is as large as >500 nm, corresponding to a coupling strength of $g > 0.28$. For metasurfaces with ENZ thicknesses of both 10 and 80 nm, the upper and lower polariton branches show a weaker dependence on the antenna length compared to the antenna array resonance without the ITO film due to the strong coupling. The lower polariton becomes weaker for metasurfaces with thicker ENZ films and is eventually not observable when the film thickness increases further, resulting in a single upper polariton resonance of the metasurface. These results are in line with the previously reported phenomenon of a single antenna-length-invariant resonance for metasurfaces with thicker ENZ films.[21,22]

We also investigate the resonance splitting for antenna–ITO metasurfaces as a function of ITO film thickness. Figure 2(d) shows the separation amount between two split resonances for metasurfaces with ITO film thicknesses of 0–90 nm, with antenna lengths of 320, 360, 400, and 440 nm, respectively. The splitting of the metasurface resonances increases as the ITO thickness increases, indicating increasing antenna–ENZ coupling strength. For an ITO thickness of 90 nm $g > 0.36$, indicating an ultrastrong coupling regime between the antenna array and the ITO–ENZ film. The lower polariton is not visible for metasurfaces with thicker ITO films.

To explore the antenna–ENZ interaction for thicker ENZ films, we investigate the role of ITO loss in the coupling properties of the antenna array and the ITO film. We use the Drude model for permittivity of the ITO film,

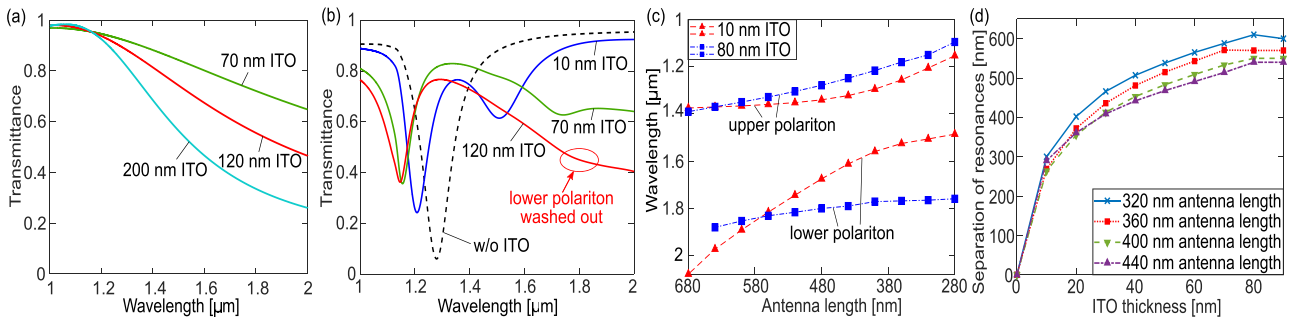

FIG. 2. (a) The simulated transmittance of the ITO films with thicknesses of 70 nm (green), 120 nm (red), and 200 nm (blue). (b) The simulated transmittance of the antenna array (black) and antenna–ITO metasurface with ITO thicknesses of 10 nm (blue), 70 nm (green), and 120 nm (red), respectively. The lower polariton is not visible in the case of 120-nm-thick ITO due to the loss of the film. (c) The wavelengths of upper and lower polaritons of the antenna–ITO metasurface for 10 nm (red) and 80 nm (blue) thicknesses of ITO films, respectively. (d) The dependence of resonance separation amount on the ITO film thickness for antenna lengths of 320 nm (blue), 360 nm (red), 400 nm (green), and 440 nm (purple), respectively.

$$\varepsilon = \varepsilon_{inf} - \frac{\omega_p^2}{\omega^2 + i\gamma\omega}, \tag{2}$$

where ω_p is the plasma frequency, ε_{inf} is the bound-electron contribution, and γ is the damping or the loss parameter of the ITO film.[2] In our simulations, we scale the γ obtained from ellipsometric measurements of a 23 nm-thick ITO film with different scaling coefficients to artificially decrease the Im(ε), corresponding to the absorption loss of the ITO film. Figure 3(a) shows the transmittance of the antenna–ITO metasurfaces with a 220 nm-thick ITO film and a 320 nm antenna length for loss parameter γ reduced by a factor of 2.5, 5, and 10, respectively. In the Drude model, γ is the loss parameter. Thus, a change in γ primarily affects the imaginary part of the permittivity. However, the real part of the permittivity is also affected by the change of γ. We find that the change of the zero-permittivity wavelength due to artificial decrease in γ is <0.6% (<8 nm). The permittivity of the ITO film with decreased γ parameter also follows the Drude model and decreasing the γ maintains the Kramers–Kronig relations between the imaginary and real parts of the permittivity. The blue curve corresponds to the metasurface with the original loss parameter of the ITO film $\gamma = 0.083\omega_p$. As shown in Fig. 3(a), for the metasurface with original ITO loss, the lower polariton is not observable due to the ITO loss, and only a single resonance corresponding to the upper polariton is visible at the wavelength of around 1120 nm [Fig. 3(a), blue curve]. When decreasing the ITO loss, the antenna–ENZ metasurface exhibits a lower polariton resonance with a large splitting of resonances. The lower polariton becomes visible as the metasurface resonances get stronger. We conclude that the antenna array and the ENZ film are in a strong coupling regime also for thicker ENZ films and the lower polariton not being observable is due to the high loss of the ENZ film. The coupling strength (i.e., resonance separation) does not increase when decreasing the loss of the ENZ film. This is because the coupling strength depends on the modal overlap and antenna resonance strength, which have a weak dependence on the loss parameter of the ITO film. Figure 3(b) shows the transmittance of antenna–ENZ metasurface with 200, 250, and 300 nm thick ITO films, respectively. The loss parameter γ is decreased 5 times. We see that in all three cases, in addition to the upper polariton resonance at a shorter wavelength, the lower polariton resonance is also visible at a longer wavelength, with large splitting of resonances. This coupling strength (i.e., splitting amount) shows a saturation when increasing the ITO thickness for this thickness range. We note that in this work, we artificially lowered the loss to uncover the underlying properties of strong coupling. In general, the loss of ITO or other similar transparent conducting oxides depends on a number of parameters, including fabrication defects, carrier concentration, and annealing temperature.[2,32–34] Thus, one will need to optimize various fabrication parameters to vary the loss of these materials.

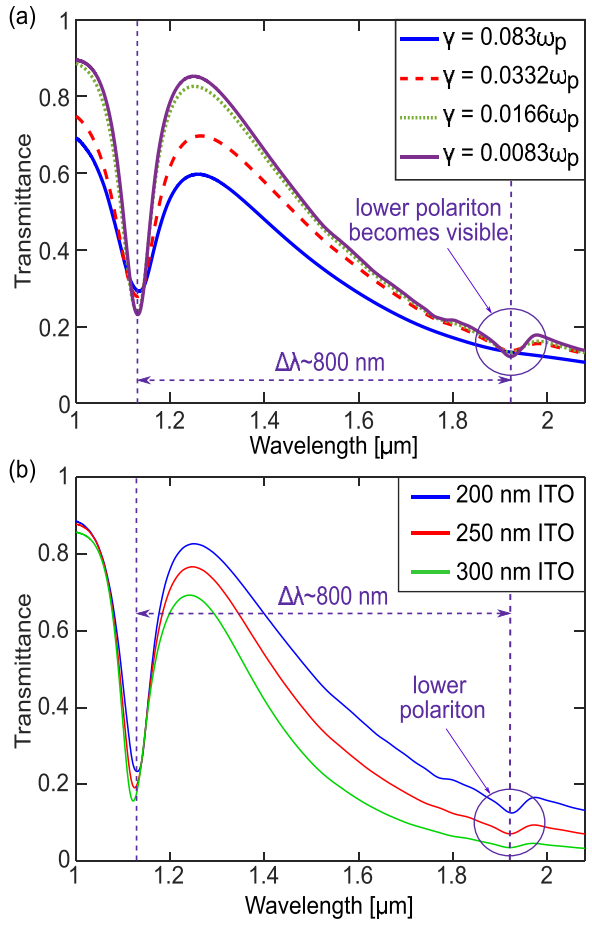

FIG. 3. (a) The simulated transmittance of the antenna–ITO metasurface with 220 nm thick ITO for the original ITO loss parameter of $\gamma = 0.083\omega_p$ (blue) and for 2.5 (red), 5 (green), and 10 (purple) times decreased γ, respectively. The lower polariton is not visible for the metasurface with the original ITO loss but becomes readily visible with a $\Delta\lambda$ resonance splitting of ~800 nm when the ITO loss is decreased. (b) The simulated transmittance of antenna–ITO metasurfaces with 200 nm, 250 nm, and 300 nm thick ITO films, respectively, for 5 times decreased γ. The splitting of resonances shows a saturation.

We also investigate the antenna–ENZ coupling strength for different ITO film thicknesses in the case of reduced ITO loss. We reduce the γ of the ITO–ENZ film five times to the value of $\gamma = 0.0166\omega_p$. Figure 4(a) shows the wavelengths of the upper and lower polariton branches for metasurfaces with ITO thicknesses of 0–300 nm and an antenna length of 320 nm. An ITO thickness of 0 nm corresponds to an antenna array without an ITO film and has a single resonance at ~1280 nm. The splitting of resonances of the antenna–ITO metasurface increases from ~400 nm to ~800 nm as the ITO thickness increases from 20 nm to 300 nm, saturating for ITO thicknesses of >180 nm. Figure 4(b) shows the dependence of the coupling strength g on the ITO film thickness. The frequency separation of the antenna–ITO metasurface resonances reaches ~30% of the zero-permittivity frequency of the ENZ film for metasurfaces with ITO–ENZ film as thin as 20 nm. The maximum separation reaches ~50% of the zero-permittivity frequency of the ENZ film, indicating an ultrastrong coupling regime between the antenna array and the ITO–ENZ film.

Furthermore, we investigate the antenna–ENZ interaction in the presence of a spacer layer between the antenna array and the ITO–ENZ film. We use a layer of SiO_2 with various thicknesses as a separation layer [Fig. 5(a)]. The antenna length and the ITO thickness are fixed to 320 and 70 nm, respectively. Figure 5(b) shows the transmittance of the antenna–ITO metasurface in the presence of such a

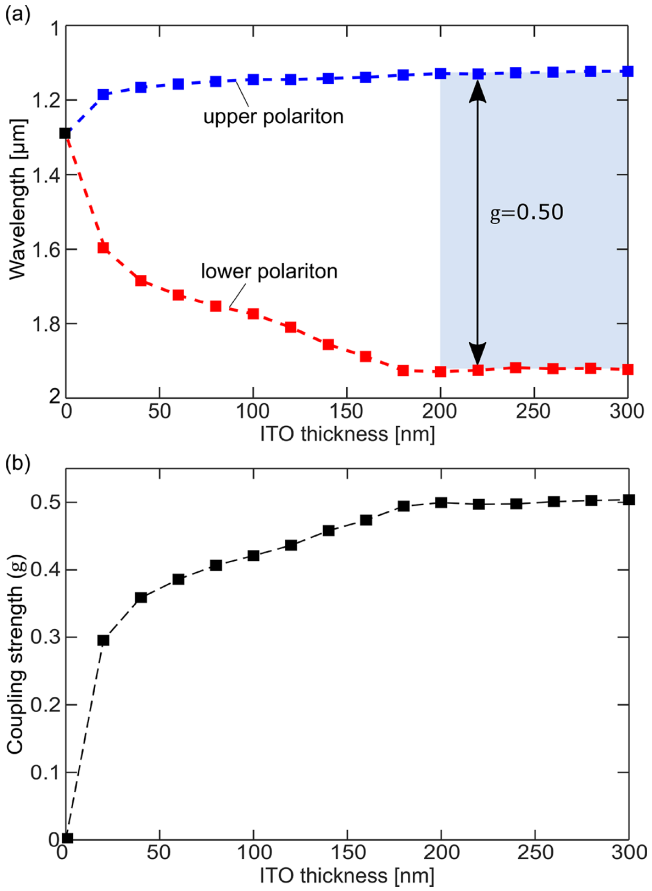

FIG. 4. (a) The resonance wavelengths of the upper (blue) and lower (red) polaritons of the antenna–ITO metasurface with reduced loss of the ITO for different ITO thicknesses. (b) The dependence of the coupling strength g on the ITO film thickness. The resonance separation increases as the thickness of the ITO–ENZ film increases, saturating for thicker ITO films in an ultrastrong coupling regime.

layer with thicknesses of 80 nm and 250 nm. The blue curve corresponds to the transmittance of the antenna–ITO metasurface with no spacer layer, and the black curve corresponds to the transmittance of the antenna array without the ITO film. For a separation distance of 80 nm, the antenna–ITO metasurface is still in a strong coupling regime, exhibiting a separation of resonances $\Delta\lambda$ of ~300 nm. An increase in the spacer layer thickness reduces the antenna–ENZ coupling, eventually making the coupling weak and merging the metasurface resonances into the resonance of the antenna array without the presence of ITO for a separation layer of 250 nm thickness.

In summary, we show that the ITO–ENZ film and the metallic antenna array are in a strong or ultrastrong coupling regime for metasurfaces with both thinner and thicker ITO–ENZ films. The lower polariton resonance is not visible for metasurfaces with thicker ENZ films and high loss of the ENZ film, resulting in a single antenna-length-invariant resonance. We also show that reducing the ENZ film loss makes the lower polariton visible, indicating an ultrastrong coupling regime for thicker ENZ films as well. The antenna–ENZ coupling becomes stronger when the ENZ film thickness increases,

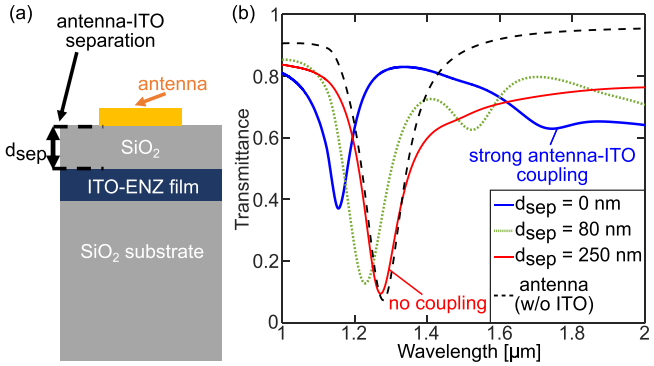

FIG. 5. (a) The structure of the antenna–ITO metasurface with a separation layer between the antenna array and the ITO film. (b) The simulated transmittance of the antenna–ITO metasurface for different separation layer thicknesses. The resonances get closer for a spacer layer thickness of 80 nm (green) and the splitting gets negligible for 250 nm separation (red), resulting in a single resonance of the antenna–ITO metasurface at the same wavelength as that of the resonance of the antenna array without an ITO film.

saturating in an ultrastrong coupling regime. Additionally, we show that the coupling becomes weaker if the antenna array and the ENZ film are spatially separated and eventually becomes negligible when separation thickness increases.

The authors would like to acknowledge the support of the Defense Advanced Research Projects Agency (DARPA) under the NLM Nascent Light-Matter Interactions program (Grant No. W911NF-18-0369).

DATA AVAILABILITY

The data that support the findings of this study are available from the corresponding author upon reasonable request.

REFERENCES

[1]S. Campione, I. Brener, and F. Marquier, "Theory of epsilon-near-zero modes in ultrathin films," Phys. Rev. B **91**, 121408 (2015).
[2]A. Capretti, Y. Wang, N. Engheta, and L. Dal Negro, "Enhanced third-harmonic generation in Si-compatible epsilon-near-zero indium tin oxide nanolayers," Opt. Lett. **40**, 1500–1503 (2015).
[3]M. Z. Alam, I. De Leon, and R. W. Boyd, "Large optical nonlinearity of indium tin oxide in its epsilon-near-zero region," Science **352**, 795–797 (2016).
[4]I. Liberal and N. Engheta, "Near-zero refractive index photonics," Nat. Photonics **11**, 149–158 (2017).
[5]S. Vezzoli, V. Bruno, C. DeVault, T. Roger, V. M. Shalaev, A. Boltasseva, M. Ferrera, M. Clerici, A. Dubietis, and D. Faccio, "Optical time reversal from time-dependent epsilon-near-zero media," Phys. Rev. Lett. **120**, 043902 (2018).
[6]O. Reshef, I. De Leon, M. Z. Alam, and R. W. Boyd, "Nonlinear optical effects in epsilon-near-zero media," Nat. Rev. Mater. **4**, 535–551 (2019).
[7]N. Kinsey, C. DeVault, A. Boltasseva, and V. M. Shalaev, "Near-zero-index materials for photonics," Nat. Rev. Mater. **4**, 742–760 (2019).
[8]Y. Zhou, M. Z. Alam, M. Karimi, J. Upham, O. Reshef, C. Liu, A. E. Willner, and R. W. Boyd, "Broadband frequency translation through time refraction in an epsilon-near-zero material," Nat. Commun. **11**, 2180 (2020).
[9]A. Baev, P. N. Prasad, M. Z. Alam, and R. W. Boyd, "Dynamically controlling local field enhancement at an epsilon-near-zero/dielectric interface via nonlinearities of an epsilon-near-zero medium," Nanophotonics **9**, 4831–4837 (2020).

[10]M. Lobet, I. Liberal, E. N. Knall, M. Z. Alam, O. Reshef, R. W. Boyd, N. Engheta, and E. Mazur, "Fundamental radiative processes in near-zero-index media of various dimensionalities," ACS Photonics **7**, 1965–1970 (2020).
[11]Y. C. Jun, J. Reno, T. Ribaudo, E. Shaner, J.-J. Greffet, S. Vassant, F. Marquier, M. Sinclair, and I. Brener, "Epsilon-near-zero strong coupling in metamaterial-semiconductor hybrid structures," Nano Lett. **13**, 5391–5396 (2013).
[12]S. A. Schulz, A. A. Tahir, M. Z. Alam, J. Upham, I. D. Leon, and R. W. Boyd, "Optical response of dipole antennas on an epsilon-near-zero substrate," Phys. Rev. A **93**, 063846 (2016).
[13]S. Campione, J. R. Wendt, G. A. Keeler, and T. S. Luk, "Near-infrared strong coupling between metamaterials and epsilon-near-zero modes in degenerately doped semiconductor nanolayers," ACS Photonics **3**, 293–297 (2016).
[14]M. Z. Alam, S. A. Schulz, J. Upham, I. D. Leon, and R. W. Boyd, "Large optical nonlinearity of nanoantennas coupled to an epsilon-near-zero material," Nat. Photonics **12**, 79–83 (2018).
[15]J. R. Hendrickson, S. Vangala, C. K. Dass, R. Gibson, J. Goldsmith, K. Leedy, D. Walker, J. W. Cleary, T. S. Luk, W. Kim *et al.*, "Plasmonic enhancement of epsilon-near-zero modes," in *Nonlinear Photonics* (Optical Society of America, 2018).
[16]V. Bruno, C. DeVault, S. Vezzoli, Z. Kudyshev, T. Huq, S. Mignuzzi, A. Jacassi, S. Saha, Y. Shah, S. Maier *et al.*, "Negative refraction in time-varying strongly coupled plasmonic-antenna–epsilon-near-zero systems," Phys. Rev. Lett. **124**, 043902 (2020).
[17]X. Niu, X. Hu, Q. Sun, C. Lu, Y. Yang, H. Yang, and Q. Gong, "Polarization-selected nonlinearity transition in gold dolmens coupled to an epsilon-near-zero material," Nanophotonics **9**, 4839–4851 (2020).
[18]C. Liu, K. Pang, K. Manukyan, O. Reshef, Y. Zhou, J. Patrow, A. Pennathur, H. Song, Z. Zhao, R. Zhang *et al.*, "Resonance splitting and enhanced optical nonlinearities in ITO-based epsilon-near-zero metasurface with cross-shaped nanoantennas," in *CLEO: QELS_Fundamental Science* (Optical Society of America, 2019), pp. FW4B-45.
[19]K. Manukyan, M. Z. Alam, C. Liu, K. Pang, H. Song, Z. Zhao, M. Tur, R. W. Boyd, and A. E. Willner, "Interaction between a nanoantenna array and an epsilon-near-zero thin film: Ultrastrong coupling and resonance pinning for engineered highly nonlinear metasurface," in *Conference on Lasers and Electro-Optics (CLEO)* (IEEE, 2020), pp. 1–2.
[20]K. Pang, M. Z. Alam, Y. Zhou, O. Reshef, C. Liu, K. Manukyan, M. Voegtle, A. Pennathur, C. Tseng, X. Su *et al.*, "Plasmonic nanoantenna-enhanced adiabatic wavelength conversion using a time-varying epsilon-near-zero-based metasurface," in *CLEO: QELS_Fundamental Science* (Optical Society of America, 2020).
[21]J. Kim, A. Dutta, G. V. Naik, A. J. Giles, F. J. Bezares, C. T. Ellis, J. G. Tischler, A. M. Mahmoud, H. Caglayan, O. J. Glembocki *et al.*, "Role of epsilon-near-zero substrates in the optical response of plasmonic antennas," Optica **3**, 339–346 (2016).
[22]C. T. DeVault, V. A. Zenin, A. Pors, K. Chaudhuri, J. Kim, A. Boltasseva, V. M. Shalaev, and S. I. Bozhevolnyi, "Suppression of near-field coupling in plasmonic antennas on epsilon-near-zero substrates," Optica **5**, 1557–1563 (2018).
[23]Y. Todorov, A. M. Andrews, R. Colombelli, S. De Liberato, C. Ciuti, P. Klang, G. Strasser, and C. Sirtori, "Ultrastrong light-matter coupling regime with polariton dots," Phys. Rev. Lett. **105**, 196402 (2010).
[24]P. Törmä and W. L. Barnes, "Strong coupling between surface plasmon polaritons and emitters: A review," Rep. Prog. Phys. **78**, 013901 (2015).
[25]E. L. Runnerstrom, K. P. Kelley, T. G. Folland, J. R. Nolen, N. Engheta, J. D. Caldwell, and J.-P. Maria, "Polaritonic hybrid-epsilon-near-zero modes: Beating the plasmonic confinement vs propagation-length trade-off with doped cadmium oxide bilayers," Nano Lett. **19**, 948–957 (2019).
[26]D. Yoo, F. de León-Pérez, M. Pelton, I.-H. Lee, D. A. Mohr, M. B. Raschke, J. D. Caldwell, L. Martín-Moreno, and S.-H. Oh, "Ultrastrong plasmon–phonon coupling via epsilon-near-zero nanocavities," Nat. Photonics **15**, 125–126 (2021).
[27]A. F. Kockum, A. Miranowicz, S. De Liberato, S. Savasta, and F. Nori, "Ultrastrong coupling between light and matter," Nat. Rev. Phys. **1**, 19–40 (2019).
[28]C. Ciuti, G. Bastard, and I. Carusotto, "Quantum vacuum properties of the intersubband cavity polariton field," Phys. Rev. B **72**, 115303 (2005).
[29]S. Vassant, J.-P. Hugonin, F. Marquier, and J.-J. Greffet, "Berreman mode and epsilon near zero mode," Opt. Express **20**, 23971–23977 (2012).
[30]P. Berini, "Long-range surface plasmon polaritons," Adv. Opt. Photonics **1**, 484–588 (2009).
[31]S. A. Maier, *Plasmonics: Fundamentals and Applications* (Springer Science & Business Media, 2007).
[32]J. Lian, D. Zhang, R. Hong, P. Qiu, T. Lv, and D. Zhang, "Defect-induced tunable permittivity of epsilon-near-zero in indium tin oxide thin films," Nanomaterials **8**, 922 (2018).
[33]N. M. Ahmed, F. A. Sabah, H. Abdulgafour, A. Alsadig, A. Sulieman, and M. Alkhoaryef, "The effect of post annealing temperature on grain size of indium-tin-oxide for optical and electrical properties improvement," Results Phys. **13**, 102159 (2019).
[34]R. Secondo, J. Khurgin, and N. Kinsey, "Absorptive loss and band non-parabolicity as a physical origin of large nonlinearity in epsilon-near-zero materials," Opt. Mater. Express **10**, 1545–1560 (2020).